THE JOURNAL OF PHYSICAL CHEMISTRY B

Article

pubs.acs.org/JPCB

Orientational Dynamics of Room Temperature Ionic Liquid/Water Mixtures: Water-Induced Structure

Adam L. Sturlaugson, Kendall S. Fruchey, and Michael D. Fayer*

Department of Chemistry, Stanford University, Stanford, California 94305, United States

ABSTRACT: Optical heterodyne detected optical Kerr effect (OHD-OKE) measurements on a series of 1-alkyl-3-methylimidazolium tetrafluoroborate room-temperature ionic liquids (RTILs) as a function of chain length and water concentration are presented. The pure RTIL reorientational dynamics are identical in form to those of other molecular liquids studied previously by OHD-OKE (two power laws followed by a single exponential decay at long times), but are much slower at room temperature. In contrast, the addition of water to the longer alkyl chain RTILs causes the emergence of a long time biexponential orientational anisotropy decay. Such distinctly biexponential decays have not been seen previously in OHD-OKE experiments on any type of liquid and are analyzed here using a wobbling-in-a-cone model. The slow component for the longer chain RTILs does not obey the Debye−Stokes−Einstein (DSE) equation across the range of solutions, and thus we attribute it to slow cation reorientational diffusion caused by a stiffening of cation alkyl tail−tail associations. The fast component of the decay is assigned to the motions (wobbling) of the tethered imidazolium head groups. The wobbling-in-a-cone analysis provides estimates of the range of angles sampled by the imidazolium head group prior to the long time scale complete orientational randomization. The heterogeneous dynamics and non-DSE behavior observed here should have a significant effect on reaction rates in RTIL/water cosolvent mixtures.

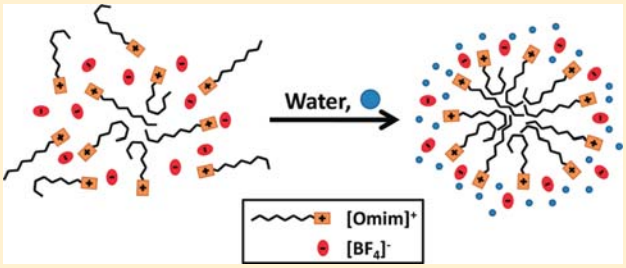

I. INTRODUCTION

Room temperature ionic liquids (RTILs), salts with a melting point below 25 °C, have garnered much interest in the past decade due to their very low volatility, enormous variability, and good thermal stability. They are often composed of an inorganic anion paired with an asymmetric organic cation which contains one or more pendant alkyl chains. The asymmetry of the cation frustrates crystallization, causing the salt's melting point to drop significantly. RTILs have applications in electrochemistry, separation processes, and organic synthesis, among others.[1]

Despite the growth in RTIL applications, there still remains a significant debate about the liquid structure of pure RTILs. For a number of years, the general consensus was that there was significant nanoscale ordering, with the long, oily hydrocarbon tails aggregating to form nonpolar domains and with the cationic head group and the anion forming tortuous ion channels that percolated through the pure liquid on relatively long length scales. Nanoscale correlation was first predicted by Urahata and Ribeiro[2] using united atom molecular dynamics (MD) simulations. Subsequent coarse-grained[3,4] and fully atomistic[5,6] MD simulations further supported the idea of nanostructural organization with simulation snapshots showing aggregation of the alkyl tails. The first experimental evidence in favor of such organization came from the X-ray scattering data of Triolo and co-workers[7−9] in which a low-Q scattering peak was seen at a length scale close to that predicted by the MD simulations. Within that framework, many successive experiments, including fluorescence,[10−12] optical Kerr effect,[13−17] and dielectric spectroscopies;[16,18] NMR;[19,20] and small-angle neutron scattering (SANS),[21] were interpreted by invoking the liquid nanostructure concept. Furthermore, anomalous reaction rates in RTILs have been attributed to this nanoscale structural heterogeneity.[22,23] However, in 2010, H/D isotope labeled SANS experiments by Hardacre[24] and MD simulations by Annapureddy and Margulis[25] showed that the low-Q peak seen in Triolo's X-ray scattering data was not due to alkyl tail correlations, but instead due to correlations of the charged groups. They argue that the low-Q peak can be explained by anisotropic solvation, in which the alkyl cation is preferentially solvated on the alkyl tail side by other alkyl tails and on the imidazolium side by anions. This leads to two first solvation shell length scales, the longer of which will give rise to the low-Q peak without needing to invoke more complex nanostructures. In contrast, recent scattering experiments by Triolo on binary mixtures of RTILs and on RTILs with polar polyether tails are interpreted as supporting the nanostructuring idea.[26] Thus, the discussion continues, with both explanations invoked in recent papers.[27−31]

The addition of cosolvents to RTILs has also gained a significant amount of attention.[32] To reduce the often detrimentally high viscosity of most RTILs, low viscosity cosolvents are frequently added.[33,34] One of the most common cosolvents, water, is especially important, in part due to the

Received: October 16, 2011
Revised: December 28, 2011
Published: January 9, 2012

hygroscopic nature of many RTILs and the significant effect a small amount of water can have on properties such as viscosity and conductivity.[35] In applications, RTILs will have some water in them because of the difficulties and expense of producing dry ionic liquids. Thus, the question of the role of water in RTILs on the liquid's structure and dynamics is of importance. Voth and co-workers simulated the addition of water to various RTILs and proposed that adding water promotes the alkyl tail aggregation up to a water mole fraction of ~0.75 and then proceeds to break it up as the volume fraction of water becomes larger.[36,37] Firestone observed that 1-decyl-3-methylimidazolium bromide or nitrate (DmImBr or $DmImNO_3$) RTILs gelled at similar mole fractions of water,[38] and Bowers noticed the same behavior for 1-methyl-3-octylimidazolium chloride (OmImCl).[39] Later, Bhargava and Klein successfully simulated the hexagonal mesophase structure originally proposed by Firestone.[40] Regardless of whether the rate of reactions in RTILs is dependent on the presence of nanostructural organization in the pure liquid, the structural changes in RTIL/water cosolvent mixtures should significantly alter reaction rates and thus the dynamics of such binary mixtures are important.

The purpose of this work is to address how the addition of water influences the dynamics and structure of RTILs. Toward this end, we have performed optically heterodyne detected optical Kerr effect (OHD-OKE) experiments on a series of 1-alkyl-3-methylimidazolium tetrafluoroborate RTILs (Figure 1)

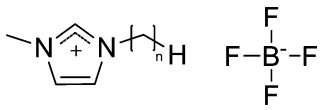

Figure 1. Structure of 1-alkyl-3-methylimidazolium tetrafluoroborate. Abbreviations used here are $BmImBF_4$, $HmImBF_4$, $OmImBF_4$, and $DmImBF_4$ for n = 4, 6, 8, and 10, respectively.

and their mixtures with water. Using a new experimental method, we follow the decays from a few hundred femtoseconds up to ~0.4 microseconds (six decades of time) and over six decades of signal amplitude. The typical data set is composed of two power law decays at shorter times followed by a final exponential decay. The pure RTIL decays are similar to those of normal molecular liquids (*o*-terphenyl, dibutylphthalate), but are an order of magnitude slower at room temperature. As water is added, the viscosities of all of the RTIL solutions decrease monotonically. For the shorter alkyl chain samples, and for the lower water concentrations of the longer chain samples, as water is added the final single exponential decay becomes faster. The final exponential decay reflects the complete randomization of the liquid structure. However, when water is added to the RTILs with an alkyl tail of hexyl or longer, the long time scale orientational dynamics become biexponential. The slowest component of the dynamics for the RTILs with octyl or decyl tails does not obey the Debye–Stokes–Einstein (DSE) equation, which we attribute to significant local structuring of the alkyl tails. The fast component of the biexponential dynamics is assigned to the restricted reorientation of the imidazolium head group (wobbling-in-a-cone). Detailed analysis yields estimates of the cone angle sampled by the head group prior to complete randomization. The biexponential dynamics and non-DSE behavior of the systems studied here indicate that the use of water as an RTIL cosolvent will have effects on reaction rates that cannot be solely explained by changes in viscosity.

II. EXPERIMENTAL PROCEDURES

1-Butyl-3-methylimidazolium tetrafluoroborate ($BmImBF_4$, 99%), 1-hexyl-3-methylimidazolium tetrafluoroborate ($HmImBF_4$, 99%), 1-methyl-3-octylimidazolium tetrafluoroborate ($OmImBF_4$, 99%), and 1-decyl-3-methylimidazolium tetrafluoroborate ($DmImBF_4$, >98%) were purchased from Iolitec and were dried under vacuum at ~55 °C for at least 24 h before being transferred to a nitrogen glovebox for storage. Pure RTIL samples were prepared in the glovebox to prevent atmospheric water uptake. RTIL/water mixtures were prepared by mass. $HmImBF_4$, $OmImBF_4$, are $DmImBF_4$ are not fully miscible with water (unlike $BmImBF_4$), saturating at a water mole fraction of ~0.75 at 24.5 °C. For this paper we define water mole fraction as moles of H_2O/(moles of cation + moles of anion + moles of H_2O). Water contents were checked by Karl Fischer titration after data acquisition for all samples with a water mole fraction of 0.76 or less. For the pure RTILs, the water concentration was 100 ppm or less. Water concentration data are shown in Table 1. Samples were filtered using 0.1–0.45 μm filter pore sizes (depending on viscosity) into optical grade cuvettes for OHD-OKE measurements. Dynamic viscosities for $BmImBF_4$ and $HmImBF_4$ solutions were taken from the literature.[41−43] Three data sets were averaged for $BmImBF_4$. For the $OmImBF_4$ and $DmImBF_4$ solutions, dynamic viscosities were measured with a Brookfield LVDV-11+P cone and plate viscometer. Multiple literature values were averaged for the pure viscosity of $OmImBF_4$,[44−49] while the pure $DmImBF_4$ viscosity was measured in the nitrogen glovebox using the Brookfield viscometer. All measurements were done at 24.5 °C. Imidazolium tetrafluoroborate RTILs are known to hydrolyze slowly in the presence of water.[50] To ensure that the measured dynamics of the binary mixtures were not affected by the hydrolysis products, the OHD-OKE decays of fresh and weeks-old samples were compared. No measurable difference was seen.

The optical Kerr effect is a nonresonant pump–probe technique in which a linearly polarized (0°) pump laser pulse induces a transient birefringence in a liquid sample. A second, linearly polarized (45°) pulse then probes the sample, emerging elliptically polarized due to the sample's pump-induced birefringence. The decay of the birefringence can be measured with femtosecond resolution by mechanically varying the pump–probe delay and is related to the orientational relaxation dynamics of the liquid (see Results). Optical heterodyne detection is incorporated with an in-phase local oscillator by placing a quarter wave plate before the sample with its fast axis aligned along the probe polarization and then slightly rotating (~3°) the probe polarization into the wave plate. This generates an elliptically polarized probe at the sample. Phase cycling is done by changing the probe polarization into the wave plate (±3°) on successive scans and subtracting the two scans. This enables removal of the homodyne signal and electrical pickup noise since they do not change sign when the probe ellipticity is flipped, while the signal does. Because the technique is nonresonant, the pulses can be chirped, allowing for higher average powers and thus greater signal at longer times. For the data presented here, up to three pulses widths were used, ~55 fs, ~2.5 ps, and ~125 ps, which allowed data collection out to 30 ps, 600 ps, and 15 ns, respectively. The various time scans overlapped over some range of times. The

Table 1. RTIL/Water Mixture DSE Parameters

sample (mole ratio RTIL:H_2O)	mole fraction H_2O[a]	% H_2O (w/w)	viscosity,[b] cP	A_1[c]	τ_1,[d] ps	τ_2,[d] ps
$BmImBF_4$:H_2O						
4550:1 (pure)	0.000220	0.00175	103[e]	–	–	1 400
27:1	0.0364	0.297	84.0[e]	–	–	1 270
14:1	0.0655	0.560	76.2[e]	–	–	1 110
6:1	0.143	1.31	55.2[e]	–	–	918
3:1	0.245	2.52	36.7[e]	–	–	677
1:1	0.500	7.38	14.0[e]	–	–	304
1:3	0.747	19.0	6.46[e]	–	–	124
1:6	0.858	32.5	3.51[e]	–	–	91
1:15	0.938	54.7	1.95[e]	–	–	65
1:30	0.968	70.7	1.44[e]	–	–	49
1:100	0.990	88.8	1.05[e]	–	–	30
$HmImBF_4$:H_2O						
722:1 (pure)	0.00138	0.00982	190[f]	–	–	3 950
16:1	0.0587	0.440	145	–	–	3 330
8:1	0.113	0.897	112	–	–	2 720
4:1	0.215	1.90	76.6	–	–	1 850
1:1	0.510	6.87	23.8	0.80	400	949
1:3 (satd)	0.755	17.9	8.98	4.73	284	699
$OmImBF_4$:H_2O						
934:1 (pure)	0.00107	0.00684	352[g]	–	–	9 980
14:1	0.0685	0.467	243	–	–	8 660
6:1	0.148	1.10	174	–	–	6 730
3:1	0.246	2.04	116	1.01	2070	6 130
1:1	0.497	5.94	54.9	4.35	1100	5 710
1:2.5 (satd)	0.716	13.9	24.2	7.06	618	6 160
$DmImBF_4$:H_2O						
822:1 (pure)	0.00121	0.00706	630	–	–	14 300
64:1	0.0153	0.0904	452	–	–	11 500
13:1	0.0708	0.440	376	–	–	10 100
6:1	0.144	0.971	294	1.28	2860	15 000
3:1	0.266	2.06	203	2.09	2240	17 300
1:1	0.522	5.96	96.0	4.76	1390	30 500
1:2.35 (satd)	0.701	12.0	57.5	5.87	777	89 000

[a]Mole fraction of water is defined here as: moles of H_2O/(moles of cation + moles of anion + moles of H_2O); error bars: <±1%. [b]Error bars for the values measured here: ±1%. [c]Error bars: ±10%. [d]Error bars: ±10%. [e]Interpolated and averaged from refs 41−43. [f]Interpolated from ref 43. [g]Interpolated and averaged from refs 44,45,47−49.

amplitudes of the scans were matched in the overlap regions. These three scans were then combined in software to produce the full OHD-OKE decay curve.

The pump and probe pulses were generated from a 5 kHz Ti:sapphire regenerative amplifier seeded by an 86 MHz Ti:sapphire mode-locked oscillator. Details of the laser and experiment are described elsewhere[51] with the only difference in this study being the use of a balanced detector in addition to the lock-in amplifier. For the sample with the slowest dynamics (water-saturated $DmImBF_4$) in which there was significant signal left after 15 ns, additional data after 15 ns were collected by placing a Pockels cell (PC) single pulse selector in the output of the oscillator and single pulse selecting to generate a new probe pulse. By selecting sequential oscillator probe pulses, OHD-OKE data were taken out to 410 ns with a resolution of 11.6 ns. To improve the signal-to-noise ratio with this setup, two additional techniques were employed. First, a spatial filter was added to the probe beam after the sample and before the analyzing polarizer. This filter consists of a 1:1 telescope (f = 1.9 cm) and a 30 μm pinhole at the waist between the lenses. The pinhole selectively passes the probe beam and not the scattered light, due to the latter's different divergence at the sample. Second, instead of chopping both the pump and the probe, PCs were placed in both beams before the sample. The probe PC flips the local oscillator phase at 2.5 kHz, replacing the mechanical scan-to-scan flipping described above, and enables shot-to-shot subtraction of the homodyne signal and electrical noise. The pump PC rotates the pump polarization 90° at 1.25 kHz. With this setup, none of the lock-in amplifier's quadrants are dominated by a scattering term, leading to an increase in dynamic range and a significant reduction in large scattering signals "bleeding" into the OHD-OKE signal quadrant due to imperfect quadrant orthogonality. In addition, the dual PC phase cycling technique gives 4 times the signal relative to dual chopping.

III. RESULTS

The optical Kerr effect measures the time derivative of the anisotropic component of the collective polarizability−polarizability correlation function. At very short times (less than a couple of picoseconds), collision-induced effects contribute to the OHD-OKE signal, but the long time portion is essentially the time derivative of the second Legendre polynomial collective orientational correlation function.[52−54] For the

dx.doi.org/10.1021/jp209942r | J. Phys. Chem. B 2012, 116, 1777−1787

RTIL/water solutions measured here, we assume that the water, since it has an exceedingly small anisotropic polarizability relative to the RTIL, gives a negligible contribution to the OHD-OKE signal.[55] In addition, by symmetry the tetrafluoroborate anion has no anisotropic polarizability; it will produce zero OHD-OKE signal except at the very shortest times when collision-induced effects can produce a weak, short-lived signal. Thus, we take the OHD-OKE decay to be the time derivative of the second Legendre polynomial collective orientational correlation function of the cation, with contributions from the imidazolium ring, and to a lesser degree the alkyl tail, as discussed below.

Figure 2 shows three representative OHD-OKE decays for three $BmImBF_4$ samples on a logarithmic plot. The curves have been offset along the vertical axis for clarity. All the $BmImBF_4$ solution OHD-OKE decays, including those not shown, have similar trends—that is, a power law at short time, a power law at intermediate time, and an exponential decay at long time. To extract the orientational decay time, the data were fit to the empirical equation

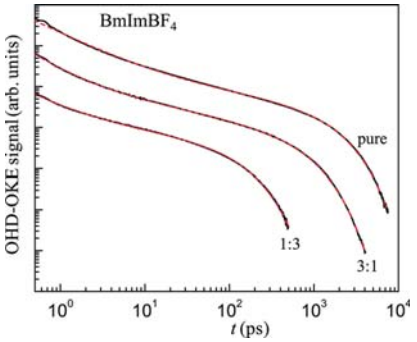

Figure 2. OHD-OKE decays for three of the $BmImBF_4$:H_2O samples (solid black curves) and their fits to eq 1 (dashed red curves). Curves have been offset along the vertical axis for clarity.

$$F(t) = [at^{-s} + dt^{b-1}] \exp(-t/\tau_2) \quad (1)$$

This general form has been seen in many other liquids[51,56−59] and has the form that results from fits with schematic mode coupling theory (MCT).[59−62] The power laws are asymptotic solutions to the MCT equations over certain time ranges and are termed the intermediate power law and the von Schweidler power law, respectively. The power laws reflect the dynamics on time scales during which a molecule is "caged" by the surrounding molecules and is not undergoing orientational diffusion. The final exponential decay corresponds to complete randomization of the orientation by orientational diffusion. Since the derivative of an exponential is the same exponential within a scaling factor, the decay time in eq 1 (τ_2) is the time constant for the decay of the slow part of the orientational correlation function. The inclusion of the power laws in the global fits are necessary to extract the correct exponential decay time. Representative OHD-OKE decays for samples with alkyl chains hexyl and longer are shown in Figures 3−5. For the higher water content, long alkyl tail samples, the OHD-OKE data could not be satisfactorily fit with eq 1.

As can be seen in Figures 4 and 5, the water-saturated samples appear to have a biexponential form (see arrows). The biexponential long time behavior is particularly clear in Figure 5. Therefore, these samples, which did not fit well to eq 1, were fit with a modified, biexponential form:

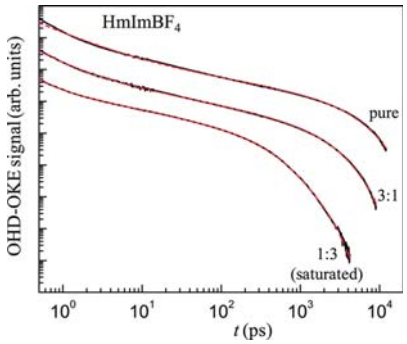

Figure 3. OHD-OKE decays for three select $HmImBF_4$:H_2O samples (solid black curves) and their fits to eq 1 or 2 (dashed red curves). Curves have been offset along the vertical axis for clarity.

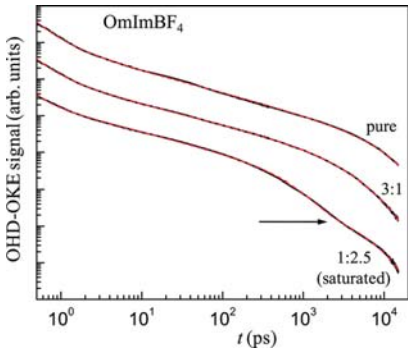

Figure 4. OHD-OKE decays for three select $OmImBF_4$:H_2O samples (solid black curves) and their fits to eq 1 or 2 (dashed red curves). Curves have been offset along the vertical axis for clarity. The biexponential decay is indicated by the arrow.

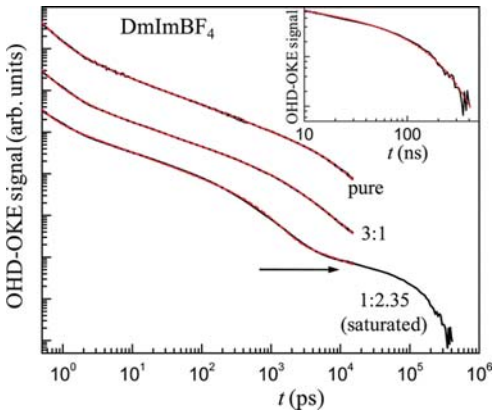

Figure 5. OHD-OKE decays for three select $DmImBF_4$:H_2O samples (solid black curves) and their fits to eq 1 or 2 (dashed red curves). Curves have been offset along the vertical axis for clarity. The inset shows the long time portion of the water-saturated $DmImBF_4$ sample and fit. Note the change in the time units. The biexponential decay is indicated by the arrow.

$$F(t) = [at^{-s} + dt^{b-1}][A_1 \exp(-t/\tau_1) + \exp(-t/\tau_2)] \quad (2)$$

Because of the large time scale covered for the water-saturated $DmImBF_4$ sample, the data were fit from 0.5 ps to 15 ns with

dx.doi.org/10.1021/jp209942r | J. Phys. Chem. B 2012, 116, 1777−1787

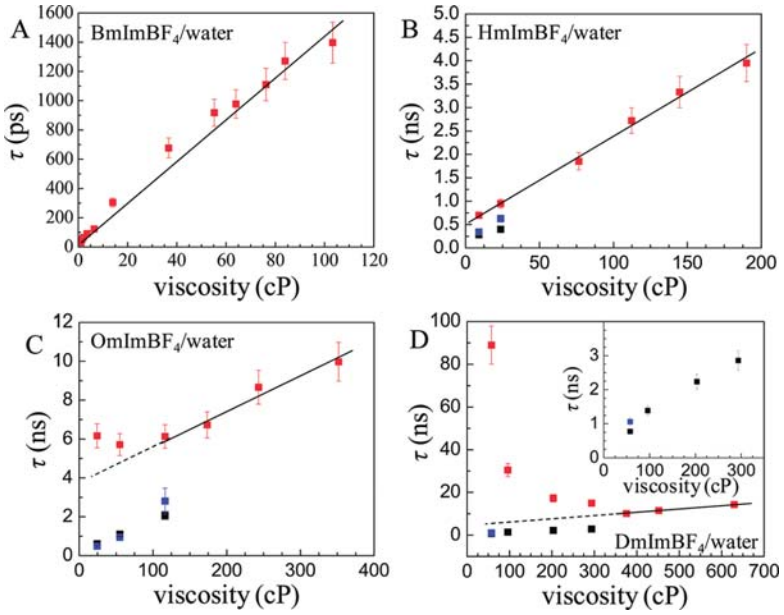

Figure 6. DSE plots for (A) $BmImBF_4$, (B) $HmImBF_4$, (C) $OmImBF_4$, and (D) $DmImBF_4$. The inset in (D) has zoomed in on the fast decays. Color coding is as follows: τ_2 (red, slow component); τ_1 (black, fast component); $(6D_c)^{-1}$ (blue, from wobbling-in-a-cone model, see below). The lines are guides to the eye.

eq 2 and from 10 ns to 410 ns with a single power law times an exponential, $F(t) = dt^{b-1} \exp(-t/\tau_2)$, to extract the two exponential decay times. All of the fits (red dashed curves) are shown in Figures 2−5 along with the experimental data (black solid curves). The inset in Figure 5 shows the long time portion of the data for the water-saturated sample and its fit. Note the difference in the units of the inset time axis. The fits reproduce the decays well over their entire range. All the exponential amplitudes and decay times from the fits are reported in Table 1. It is notable that such clearly separated biexponential decays (see Figure 5) as reported here have never been seen before in optical Kerr experiments. Prior experiments on simple molecular liquids, RTILs (including those with dissolved salts), supercooled liquids, liquid crystals in their isotropic phase, and other molecules in aqueous solutions have always shown a long time scale single exponential decay preceded by the power laws.[51,56,57,59]

Biexponential decays of orientational correlation function are generally recognized as arising from one of two physical situations. In the first case, there are two separate subensembles in the sample that reorient at different rates. The fast component of the biexponential corresponds to the randomization of the fast subensemble's orientations, which leaves behind the decay of the slow subensemble's orientations. Each subensemble completely randomizes. This mechanism would require two distinct and well-defined local structures that each give rise to a single exponential decay of its orientational anisotropy. Since the vast majority of the signal comes from the imidazolium head groups (see below), for this model to be true in the systems studied here, there would have to exist two imidazolium subensembles with distinctly different dynamics due to distinctly different environments. However, the volume fraction of water in the samples showing biexponential orientational decays is ∼5% or less. It seems physically unreasonable that such a small amount of water can perturb the system to the point of generating two distinct cation subensembles with dynamics that differ by 2 orders of magnitude. Such a scenario is physically unrealistic.

The alternative case is one in which there is a single ensemble that undergoes orientational relaxation with two time scales, one fast and restricted, and one slow and complete. This is known as wobbling-in-a-cone (WC).[63,64] In this model, the fast rotational diffusion component is restricted in a potential cone, while the cone itself rotationally diffuses on a slower time scale. The functional form of the correlation function is given by

$$C_2(t) = [S^2 + (1 - S^2) \exp(-t/\tau_c)] \exp(-t/\tau_m) \quad (3)$$

where τ_c is the decay time of the diffusion within the cone, τ_m is the decay time of complete diffusive reorientational relaxation, and S^2 is termed the order parameter. Within this model, the fast decay time extracted with eq 2, τ_1, is not the cone-restricted decay time, but is related to it by

$$\tau_c^{-1} = \tau_1^{-1} - \tau_2^{-1} \quad (4)$$

and the cone semiangle, θ, is obtained using

$$S^2 = \left[\frac{1}{2} \cos\theta(1 + \cos\theta)\right]^2 \quad (5)$$

S^2 obeys the inequality $0 \le S^2 \le 1$, with $S^2 = 1$ corresponding to a cone semiangle of 0° (no cone) and $S^2 = 0$ giving a cone semiangle of 180° (unrestricted reorientation). As can be seen from eq 3, S^2 is the amplitude of the slow decay. While the diffusion constant of the final orientational randomization is given by $D_m = (6\tau_m)^{-1}$, the diffusion constant of the cone-restricted motions (hereafter referred to as the WC diffusion

dx.doi.org/10.1021/jp209942r | J. Phys. Chem. B 2012, 116, 1777−1787

constant) depends on the cone angle and is given by the expression

$$D_c = \frac{x^2(1+x_c)^2\{\ln[(1+x_c)/2] + (1-x_c)/2\}}{\tau_c(1-S^2)[2(x_c-1)]} + \frac{(1-x_c)(6+8x_c - {x_c}^2 - 12{x_c}^3 - 7{x_c}^4)}{24\tau_c(1-S^2)} \quad (6)$$

where $x = \cos\theta$. Because of this complex dependence on θ, it is not meaningful to directly compare τ_c values, but instead comparison should be made of D_c, which therefore requires knowledge of S^2. The WC model is often applied to systems in which the rotating species is tethered to a slow or immovable scaffold, such as a protein backbone[65] or a polymer chain.[66] As will be discussed below, we use the WC model to analyze the biexponential decays seen with the higher water content mixtures.

A standard way to analyze the rotational diffusion times is through the Debye−Stokes−Einstein (DSE) equation,[67] which for a symmetric top in the rotational diffusion limit is

$$\tau_{self} = \frac{\eta V}{kT} f_\theta \quad (7)$$

where τ_{self} is the rotational diffusion self-correlation time, η is the shear viscosity, V is the volume of the particle, k is Boltzmann's constant, T is the absolute temperature, and f_θ is a shape-dependent friction factor that includes the boundary condition.[68−71] The OHD-OKE experiment measures the collective correlation function, while the DSE equation applies to only self-correlations. The two times (collective vs self) are related by[72]

$$\tau_{collective} = \frac{g_2}{j_2}\tau_{self} = \frac{g_2 \eta V f_\theta}{j_2 kT} \quad (8)$$

where g_2 is the static orientational correlation factor and j_2 is the dynamic orientational correlation factor. g_2 represents the equilibrium degree of ordering in the liquid, such as nematic ordering in the nematic phase of a liquid crystal. For no orientational correlation $g_2 = 1$, but for any degree of correlation or anticorrelation $g_2 > 1$. In many cases, $g_2 \approx 1$.[52,73] Also, it is often assumed $j_2 \approx 1$, which is borne out for acetonitrile, chloroform, carbon disulfide, and benzene.[74,75] Thus, the OHD-OKE exponential decay time is often taken to be the orientational diffusion self-correlation time. While the DSE equation is hydrodynamic, it works remarkably well for describing the rotational motion of molecules.[76−78] All of the OHD-OKE exponential decay times from the fits are plotted versus viscosity in Figure 6, and the decay times are taken to be τ_{self}.

For all the RTILs studied here, the addition of water reduces the shear viscosity of the solution. As can be seen in Figure 6A, the long time scale exponential decays in the $BmImBF_4$/water samples essentially show DSE behavior. The line through the points is an aid to the eye. As the viscosity of the solution decreases, due to the addition of water, the rotational diffusion time becomes correspondingly faster, with a value of 1.4 ns for the pure RTIL and 30 ps for the most dilute solution (1:100 $BmImBF_4$:H_2O). For the next longest chain RTIL, $HmImBF_4$, the DSE relation is also obeyed for the slowest exponential (Figure 6B), but now there is a second, faster exponential relaxation process seen in the 1:1 and water-saturated samples. These are the black squares in Figure 6B−D. The blue squares in Figure 6 come from analysis using the WC model discussed previously and further below. Figure 6C shows the DSE plot for $OmImBF_4$. Similar to the $HmImBF_4$ system, there is a fast exponential rotational diffusion time that emerges for the water-rich samples (3:1, 1:1, and water-saturated, black squares). At low water content, the $OmImBF_4$ samples are fit to eq 1 (single exponentials at long time) and display DSE behavior (Figure 6C, red points at high viscosities). However, as the water content is increased, the long time decays become biexponential (see Figure 4, bottom curve). The fast component (black points) still has DSE dynamics; however, the slow component of the biexponential fits appears to plateau and possibly turn up as water is added. Thus, while the viscosity is decreasing upon water addition, the slow rotational diffusion time is not affected in the water-rich samples in a manner consistent with the DSE equation.

This non-DSE behavior becomes much more dramatic in the $DmImBF_4$ plots shown in Figure 6D. Again, the rotation time for the water-poor $DmImBF_4$ samples (red squares, solid line) is single exponential. The slow single exponential and the fast component of the water-rich samples (black squares and inset) are linear in viscosity. However, the slow rotation time of the biexponential decays in the water-rich samples now moves in the opposite direction from that predicted by the DSE equation. As water is added the viscosity is going down, and yet the slow component of the rotational dynamics is drastically slowing down. For the water-saturated $DmImBF_4$, the slow component is 89 ns, while the fast component is only 780 ps. The pure (no water) $DmImBF_4$ has a long time single exponential rotational diffusion time of 14.3 ns. As can be seen in Table 1, the amplitude of the slow component grows upon addition of water and the concentration at which the biexponential behavior emerges shifts to lower water concentrations as the alkyl tail length increases.

IV. DISCUSSION

IV.1. Pure RTILs. The pure RTIL data fit well to eq 1, which is a semiempirical function based on schematic mode coupling theory and has been used to successfully model the OHD-OKE response of a wide variety of liquids.[56,59,61,62] Schematic mode coupling theory applied to OHD-OKE data consists of two coupled correlation functions: one for the density fluctuations and one for the orientational relaxation. Each correlation function consists of a damped harmonic oscillator with a memory function.[60,61] Implicit in MCT is an assumption of a homogeneous medium. There is nothing in the MCT results that corresponds to different regions with distinct structural and dynamical properties. The fact that the OHD-OKE decays reported here for the pure RTILs have the identical form as previous OHD-OKE studies of many other liquids which are not nanostructured and can be described well by the application of the MCT-based eq 1[51,58,60,61] suggests that if any nanostructuring is present, it does not have any unique effect on the rotational diffusion of the cation.

The OHD-OKE decays demonstrate one additional fact: the time scale of complete orientational randomization is long compared with those of other "normal" organic liquids at room temperature, such as dibutylphthalate or benzene.[79,80] The nanosecond or longer rotation times measured here are similar to other RTIL rotational diffusion OHD-OKE measurements[56,81] and probe solvation and rotation times from time-resolved fluorescence studies.[82−84] As evidenced by the much

smaller rotation times and viscosities of analogous alkylimidazoles,[85,86] the strong Coulombic forces present in alkylimidazolium RTILs significantly slow down the liquid dynamics, causing the red-edge effect seen in many fluorescence experiments.[87,88] The slow reorientation time puts a lower boundary on the time of solvation shell exchange, which in turn leads to relatively long-lasting cation tail−tail associations. Thus, any alkyl tail associations in the pure RTIL, whether considered nanostructured or not, will be disrupted much more slowly than in a conventional molecular liquid such as dibutylphthalate.

IV.2. RTIL/Water Mixtures. Similar to the pure RTILs, the OHD-OKE decays for RTILs with a small amount of water fit well to eq 1, with the longest time component a single exponential. The single exponential decays also follow DSE behavior up to the water content for the longer chains at which the long time relaxation becomes biexponential. It is believed that, at low concentrations, water is isolated in tetrafluoroborate and hexafluorophosphate imidazolium RTILs and is symmetrically hydrogen bonded to two anions.[89] Further addition of water screens the ions and "lubricates" them, speeding up the dynamics and lowering the solution viscosity.[90] Given the DSE behavior for these water-poor solutions, it appears that a very small amount of water does not significantly disrupt the liquid structure.

For more hydrophilic long chain imidazolium RTILs, such as OmImCl, DmImBr, or DmImNO$_3$, a sufficient amount of water induces a phase change and the sample spontaneously gels.[38−40] The concentration range over which this has been observed is 5−40% water (w/w). None of the samples prepared here showed any sign of gelation, presumably because the alkyl chain of BmImBF$_4$ is too short and because the longer chain RTILs are too hydrophobic to gel before they phase separate (see Table 1).

Given this tendency of some imidazolium RTILs to organize upon addition of a sufficient amount of water, we interpret the biexponential OHD-OKE decays as evidence for the rigidification of the imidazolium tail associations, which would presumably lead to gelation if higher water concentrations could be reached. A number of observations from the OHD-OKE data support this argument. First, the slow reorientation time from the biexponential fit, τ_2, does not decrease linearly in the viscosity; instead it plateaus (Figure 6C) or increases (Figure 6D). Given eq 8, there are a few ways in which one can get this type of non-DSE behavior. First, as water is added, g_2 could increase, indicating an increase in equilibrium correlation of cations. Due to the cation's hydrophobic tail, this seems unlikely unless there is concurrent aggregation of the alkyl tails. Second, one can imagine that the volume of the rotator increases, potentially due to stable ion pairs or clusters or due to hydrophobic-effect driven aggregation of the alkyl tails. Ion pairing effects can be ruled out through a couple considerations. First, dielectric spectroscopy has shown that in pure BmImBF$_4$ there is no evidence of significant ion pairing.[91] Additionally, conductivity measurements of BmImBF$_4$/water mixtures show that water promotes the dissociation of the ions.[92] Thus, we believe that ion pairing effects are not significant in these samples and that the slow component of the biexponential dynamics cannot be attributed to them. Given these considerations, it seems reasonable to conclude that the local cation tail−tail association has been stiffened, effectively causing two or more cations to become at least partially locked to each other and to rotate cooperatively as one larger species.

A third way to see non-DSE behavior is if j_2 became significantly smaller, due to a large transfer of angular momentum between adjacent rotators.[93] This would imply close, but loosely held, cation−cation association. However, j_2 has never been observed to deviate significantly from 1, presumably due to more efficient momentum transfer into translational modes.[73,75] While the friction factor could mathematically also cause an increase in $\tau_{collective}$, no physically realistic combination of boundary condition and shape could yield frictions as large as is needed to reproduce the DSE data presented here. Thus, it is reasonable that the trends seen in the DSE plots (Figure 6) are due to a local structuring and stiffening of the alkyl tail associations.

A second argument in favor of stiffer alkyl tail associations is based on the ratio of the amplitudes of the biexponential components. OHD-OKE measures the anisotropic component of the polarizability−polarizability correlation function. Since the aromatic ring is much more anisotropically polarizable than the alkyl tail, the majority of the signal should come from the imidazolium head. Also, if the alkyl tails are more tightly held by other alkyl tails, the imidazolium heads will be relatively free to rotate in the water-diluted ionic region of the mixture and should have a faster reorientation time. As can be seen from Table 1, the faster OHD-OKE component does have the larger amplitude. To further support this idea, we measured two additional OHD-OKE decays under identical laser conditions (16 mW, ~2.5 ps pulses, scanned to 600 ps). The first was the water-saturated OmImBF$_4$ sample, which has a viscosity of 24.2 cP. To approximate the alkyl portion of the RTIL, the second sample was light paraffin oil heated to 40 °C (24 cP). These decays are plotted in Figure 7. Since both of these samples have

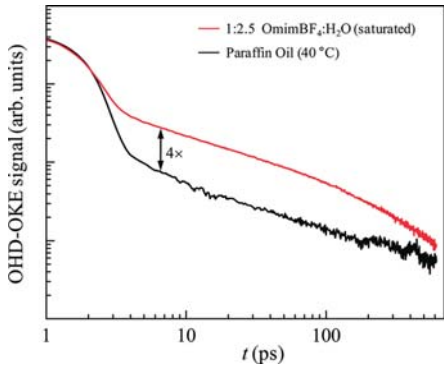

Figure 7. OHD-OKE decays comparing the signal strength from two isoviscous samples. The RTIL:H$_2$O sample gives a significantly stronger signal than a pure alkane, demonstrating a stronger OHD-OKE response from the imidazolium head than from the alkyl tail.

the same viscosity, the initial amplitudes of the OHD-OKE decays can be compared to see how much larger the RTIL signal is relative to that for a pure alkane. Figure 7 demonstrates that the RTIL:H$_2$O amplitude is about 4 times larger than that of the alkane. Simple volume arguments based on the density of the two samples and partial molecular volumes indicate that the imidazolium head gives an OHD-OKE signal about 8.3 times larger than that of the octyl tail. By scaling according to the alkyl tail volume, the signal ratios from the hexyl and decyl side chains were determined to be 11 and 6.4, respectively. These values are close to the biexponential fit amplitudes reported in Table 1 and further support the idea that the imidazolium head

group rotation corresponds to the fast decay and the local alkyl tail organization gives rise to the slow decay.

For all samples, the viscosity decreases monotonically as water is added. At first glance, this may appear to be in contradiction to the long time scale orientational relaxation of the $OmImBF_4$ and $DmImBF_4$ samples. At high water contents, the slowest orientational relaxation component of these samples is not hydrodynamic (see Figure 6). This is particularly clear for $DmImBF_4$; at high water contents, the long time component of the orientational relaxation actually slows with additional water, but the viscosity decreases. This behavior can be rationalized qualitatively by noting that viscosity is determined by both rotational and translational motions and by their coupling. As Ediger points out, for dynamically heterogeneous systems the translational diffusion constants are more sensitive to faster-than-average motions while rotational decay times emphasize slower-than-average motions.[94] Thus, if the viscosity has a greater dependence on the translation than on the rotation and if the system is dynamically heterogeneous, it is possible for the viscosity (as determined by rotational *and* translational motions) to decrease although the rotational dynamics slow.

If the assignment of the fast (head group) and slow (constrained alkyl tail) decays is correct, it is clear that the imidazolium head group is not completely free to rotate through all angles as it is tethered to the alkyl tail. Thus, its rotation is better described by the WC model discussed above. There are a number of complications that prevent one from directly fitting the OHD-OKE data to eq 3 to determine the order parameter, S^2. First, the power laws, which are attributed to caging effects, are not diffusive and therefore are not taken into account by the WC model. Second, the WC model strictly applies to one species with two time scales of motion. Here, if the assignment of the fast motions to the tethered imidazolium head group and the slow motions to the entire cation (head group and alkyl tail) is correct, then the diffusive motions contributing to the OHD-OKE signal are essentially comprised of two species with coupled dynamics. The imidazolium head group undergoes the fast, cone-limited motions, decaying to leave the overall relaxation of the cone, which is comprised of both the head group and the alkyl tail motions. Thus, one needs to know the relative signal strengths from the imidazolium ring and the alkyl tail to determine the amplitude of the final, complete decay. Third, determination of S^2 is also complicated by the fact that the OHD-OKE signal is the derivative of the correlation function and is not necessarily normalized at the correlation function level.

Due to the large separation of time scales in the water-saturated $DmImBF_4$ data, the cone angle and the WC diffusion constant were reasonably determined using the following procedure. First, the data were normalized at the correlation function level by setting the integral of the OHD-OKE data equal to 1. The electronic response in the OHD-OKE data obscures the signal at times less than ~500 fs, and will make a non-negligible contribution to the integral value. To estimate the correct normalization constant, the integration was done for two cases, one starting at 0 fs and one at 500 fs. The two normalization constants obtained this way differed by ~10%. The long time portions of the two resulting data sets were fit with a single exponential function of the form

$$F(t) = \frac{A_2}{\tau_2}\exp(-t/\tau_2) \tag{9}$$

where the prefactor accounts for the derivative nature of the OHD-OKE signal. This fitting was done with multiple starting points ranging from 10 to 55 ns. The order parameter, S^2, can then be obtained from the amplitude of the fit to eq 9 by

$$A_2 = \frac{RS^2 + 1}{R + 1} \tag{10}$$

where R is the imidazolium to decyl tail signal ratio of 6.4 (see Table 2). To account for the uncertainty in the signal ratio, R was varied ±1. By varying the normalization constant, the fit start time, and the head/tail signal ratio, over a hundred values of S^2 were obtained and used to a calculate a cone angle of 41 ± 1° and an inverse WC diffusion constant of 6.4 ± 0.7 ns. These data are listed in Table 2. Because of the large time scale separation, the amplitude, A_2, from the various fits to eq 9 did not vary much and θ and D_c have relatively small errors. Data for the other $DmImBF_4$ samples were not collected past 15 ns, and these signals do not decay completely during that experimental time window. Therefore, it was not possible to do a similar analysis on these samples. For the three $OmImBF_4$ and two $HmImBF_4$ data sets which show biexponential behavior, the procedure described above was followed with the exception of replacing eq 9 with the biexponential function

$$F(t) = \frac{A_1}{\tau_1}\exp(-t/\tau_1) + \frac{A_2}{\tau_2}\exp(-t/\tau_2) \tag{11}$$

in which the fit starting points ranged from 100 ps to 10 ns, depending on the sample. For the samples in which the reorientation time scales are not well separated (particularly the $HmImBF_4$ samples), this biexponential form was necessary to get reasonable amplitudes, A_2, of the slow decay term. The cone angles for these samples are much larger than those for the water-saturated $DmImBF_4$, ranging from 53 ± 3° to 70 ± 7°. The larger error in these values is primarily due to the uncertainty in the determination of A_2. All the wobbling-in-a-cone parameters obtained from this procedure are listed in Table 2.

Table 2. RTIL/Water Mixture Wobbling-in-a-Cone Parameters[a]

sample (mole ratio RTIL:H_2O)	OHD-OKE signal ratio (imidazolium/alkyl tail)	"effective" cone angle θ, deg	$1/D_c$, ns
$HmImBF_4$:H_2O	11		
1:1		53 ± 3	3.8 ± 0.5
1:3 (satd)		68 ± 13	2.1 ± 0.4
$OmImBF_4$:H_2O	8.3		
1:2.5 (satd)		68 ± 9	3.0 ± 0.4
1:1		70 ± 7	5.7 ± 0.6
3:1		56 ± 11	17 ± 4
$DmImBF_4$:H_2O	6.4		
1:2.35 (satd)		40 ± 1	6.4 ± 0.7

[a]Errors are the standard deviation from >100 fits.

To the best of our knowledge, the WC model has not been applied previously to OHD-OKE data, and its application as presented here requires some comments. First, because the power laws were neglected in obtaining the order parameter, the resulting cone angle and WC diffusion constant describe all motions (both diffusive and nondiffusive, i.e., caging) that are not part of the overall, final, diffusive relaxation. Second, in

principle, the asymmetry of the cation should lead to three distinct WC diffusion constants and cone angles corresponding to the three elements of the diagonalized rotational diffusion tensor. Often, as is the case here, the corresponding exponential decays are not resolvable and one obtains an average diffusion constant instead. Given these considerations, the cone angles presented here are probably better termed "effective" cone angles and describe the average potential cone in which both nondiffusive and fast diffusive reorientational dynamics occur. The WC analysis clearly contains approximations, but it is useful to rationalize trends and to provide comparisons between the various liquid systems studied.

Due to the relatively large error in θ for the $HmImBF_4$ and $OmImBF_4$ samples, it is not possible to conclusively establish trends. One would expect that as water is added to the system it would screen the cation−anion attractions, allowing the imidazolium head group more freedom to rotate, thereby increasing the cone angle. However, if the alkyl tail associations are also beginning to stiffen upon addition of water, there should be a competing drive to decrease the cone angle as the cation tails pack together and limit the imidazolium's motions. While the error bars on the data do not allow one to conclusively say this behavior is followed, the data are not inconsistent with such an interpretation. The more locally structured, long-chain $DmImBF_4$ sample has a smaller cone angle than the $OmImBF_4$ and $HmImBF_4$ samples, and the shorter chain samples indicate an increase in cone angle as water is added.

Finally, the WC diffusion constants obtained from the preceding analysis are shown in DSE fashion in Figure 6 as the blue squares. They are plotted as $(6D_c)^{-1}$ for ease of comparison with the other decay times. While the effective cone angles do affect the values, the trends for the $HmImBF_4$ and $OmImBF_4$ remain the same, and the DSE equation appears to be followed; that is, the fast rotational component of the dynamics speeds up as the viscosity of the solutions is decreased through addition of water.

If this local cation tail structuring and stiffening proposal is correct, it should have a significant influence on reaction rates in RTIL/water cosolvent mixtures. Polar reactants, which will preferentially reside in the ionic/water regions, will presumably be able to diffuse and react much faster than nonpolar reactants whose motions will be hindered by the stiffening of the alkyl tail region. Given the hygroscopic nature of many RTILs, including imidazolium tetrafluoroborates,[35] and the relatively low water concentration in $DmImBF_4$ at which the biexponential dynamics emerge (~1% w/w, see Table 1), even atmospheric water uptake could potentially alter reaction rates in RTIL/water cosolvent mixtures.

V. CONCLUDING REMARKS

We have presented the results of optically heterodyne detected optical Kerr effect experiments on a series of pure 1-alkyl-3-methylimidazolium tetrafluoroborate RTILs and their mixtures with water. The pure RTIL dynamics are identical in form to many other molecular liquids studied by OHD-OKE previously, with power laws at early time followed by an exponential relaxation at long time, and can be fit to an MCT-based function that assumes a homogeneous system. However, unlike molecular liquids, the orientational dynamics of the RTILs are very slow at room temperature. Thus, solvation shell exchange in pure RTILs is comparatively slow and alkyl tail−tail associations are disrupted slowly, regardless of whether such tail−tail associations give rise to nanostructural organization or not.

In contrast to the pure RTILs, once a sufficient amount of water is added, the mixtures show distinctly biexponential OHD-OKE decays, which we interpret as a local stiffening of the cation's alkyl tail−tail associations. The biexponential dynamics are particularly prominent in the water-saturated $DmImBF_4$ sample in which a very pronounced separation of time scales is observed (see Figure 5). We attribute the fast component to the wobbling-in-a-cone motions of the tethered imidazolium head groups and the slow component to slow, overall cation reorientation due to alkyl tail aggregates. The local stiffening of the alkyl tail associations prevents orientational relaxation of the head groups and tails on a single time scale. The cone angles for the wobbling imidazolium head groups were determined. The details of the observed dynamics, that is, the biexponential decays at higher water contents, is consistent with the water-induced gelation seen in a few other alkylmethylimidazolium RTILs,[38−40] but the solutions studied here phase separate before a gelation concentration is reached. The local structuring and stiffening of the alkyl tail associations indicate that reaction rates in RTIL/water cosolvent mixtures should be highly dependent on the nature of the reactants and not solely on the global viscosity of the mixture.

AUTHOR INFORMATION

Corresponding Author

*E-mail: fayer@stanford.edu.

ACKNOWLEDGMENTS

The authors are grateful for financial support from the National Science Foundation (DMR 0652232), the Department of Energy (DE-FG03-84ER13251), and the Air Force Office of Scientific Research (FA9550-08-1-0306).

REFERENCES

(1) Forsyth, S. A.; Pringle, J. M.; MacFarlane, D. R. *Aust. J. Chem.* **2004**, *57*, 113.
(2) Urahata, S. M.; Ribeiro, M. C. C. *J. Chem. Phys.* **2004**, *120*, 1855.
(3) Wang, Y.; Voth, G. A. *J. Am. Chem. Soc.* **2005**, *127*, 12192.
(4) Bhargava, B. L.; Devane, R.; Klein, M. L.; Balasubramanian, S. *Soft Matter* **2007**, *3*, 1395.
(5) Canongia Lopes, J. N.; Pádua, A. a. H. *J. Phys. Chem. B* **2006**, *110*, 3330.
(6) Gomes, M. F. C.; Lopes, J. N. C.; Padua, A. A. H. *Top. Curr. Chem.* **2009**, *290*, 161.
(7) Russina, O.; Triolo, A.; Gontrani, L.; Caminiti, R.; Xiao, D.; Hines, L. G.; Bartsch, R. A.; Quitevis, E. L.; Pleckhova, N.; Seddon, K. R. *J. Phys.: Condens. Matter* **2009**, *21*, No. 424121.
(8) Triolo, A.; Russina, O.; Bleif, H. J.; Di Cola, E. *J. Phys. Chem. B* **2007**, *111*, 4641.
(9) Triolo, A.; Russina, O.; Fazio, B.; Triolo, R.; Di Cola, E. *Chem. Phys. Lett.* **2008**, *457*, 362.
(10) Sarkar, A.; Trivedi, S.; Baker, G. A.; Pandey, S. *J. Phys. Chem. B* **2008**, *112*, 14927.
(11) Guo, J.; Baker, G. a.; Hillesheim, P. C.; Dai, S.; Shaw, R. W.; Mahurin, S. M. *Phys. Chem. Chem. Phys.* **2011**, *13*, 12395.
(12) Funston, A. M.; Fadeeva, T. A.; Wishart, J. F.; Castner, E. W. Jr. *J. Phys. Chem. B* **2007**, *111*, 4963.
(13) Xiao, D.; Rajian, J. R.; Cady, A.; Li, S.; Bartsch, R. A.; Quitevis, E. L. *J. Phys. Chem. B* **2007**, *111*, 4669.
(14) Xiao, D.; Rajian, J. R.; Hines, L. G. Jr.; Li, S.; Bartsch, R. A.; Quitevis, E. L. *J. Phys. Chem. B* **2008**, *112*, 13316.
(15) Xiao, D.; Rajian, J. R.; Li, S.; Bartsch, R. A.; Quitevis, E. L. *J. Phys. Chem. B* **2006**, *110*, 16174.

(16) Turton, D. A.; Hunger, J.; Stoppa, A.; Hefter, G.; Thoman, A.; Walther, M.; Buchner, R.; Wynne, K. *J. Am. Chem. Soc.* **2009**, *131*, 11140.
(17) Yang, P.; Voth, G. a.; Xiao, D.; Hines, L. G.; Bartsch, R. a.; Quitevis, E. L. *J. Chem. Phys.* **2011**, *135*, 034502.
(18) Mizoshiri, M.; Nagao, T.; Mizoguchi, Y.; Yao, M. *J. Chem. Phys.* **2010**, *132*, No. 164510.
(19) Imanari, M.; Uchida, K. I.; Miyano, K.; Seki, H.; Nishikawa, K. *Phys. Chem. Chem. Phys.* **2010**, *12*, 2959.
(20) Chiappe, C. *Monatsh. Chem.* **2007**, *138*, 1035.
(21) Atkin, R.; Warr, G. G. *J. Phys. Chem. B* **2008**, *112*, 4164.
(22) Tiwari, S.; Khupse, N.; Kumar, A. *J. Org. Chem.* **2008**, *73*, 9075.
(23) Castner, E. W.; Margulis, C. J.; Maroncelli, M.; Wishart, J. F. *Annu. Rev. Phys. Chem.* **2011**, *62*, 85.
(24) Hardacre, C.; Holbrey, J. D.; Mullan, C. L.; Youngs, T. G. A.; Bowron, D. T. *J. Chem. Phys.* **2010**, *133*, 074510.
(25) Annapureddy, H. V. R.; Kashyap, H. K.; De Biase, P. M.; Margulis, C. J. *J. Phys. Chem. B* **2010**, *114*, 16838.
(26) Russina, O.; Triolo, A. *Faraday Discuss.* **2011**, *154*, 97.
(27) Aoun, B.; Goldbach, A.; Gonzalez, M. A.; Kohara, S.; Price, D. L.; Saboungi, M. L. *J. Chem. Phys.* **2011**, *134*, No. 104509.
(28) Macchiagodena, M.; Gontrani, L.; Ramondo, F.; Triolo, A.; Caminiti, R. *J. Chem. Phys.* **2011**, *134*, No. 114521.
(29) Kashyap, H. K.; Santos, C. S.; Annapureddy, H. V. R.; Murthy, N. S.; Margulis, C. J.; Castner, E. W. *Faraday Discuss.* **2012**, *154*, 133.
(30) Santos, C. S.; Murthy, N. S.; Baker, G. A.; Castner, E. W. *J. Chem. Phys.* **2011**, *134*, No. 121101.
(31) Santos, C. S.; Annapureddy, H. V. R.; Murthy, N. S.; Kashyap, H. K.; Castner, E. W.; Margulis, C. J. *J. Chem. Phys.* **2011**, *134*, No. 064501.
(32) Dupont, J.; de Souza, R. F.; Suarez, P. A. Z. *Chem. Rev.* **2002**, *102*, 3667.
(33) Khupse, N. D.; Kumar, A. *J. Phys. Chem. A* **2011**, *115*, 10211.
(34) Khupse, N. D.; Kumar, A. *J. Solution Chem.* **2009**, *38*, 589.
(35) Ries, L. A. S.; do Amaral, F. A.; Matos, K.; Martini, E. M. A.; de Souza, M. O.; de Souza, R. F. *Polyhedron* **2008**, *27*, 3287.
(36) Feng, S.; Voth, G. A. *Fluid Phase Equilib.* **2010**, *294*, 148.
(37) Jiang, W.; Wang, Y. T.; Voth, G. A. *J. Phys. Chem. B* **2007**, *111*, 4812.
(38) Firestone, M. A.; Rickert, P. G.; Seifert, S.; Dietz, M. L. *Inorg. Chim. Acta* **2004**, *357*, 3991.
(39) Bowers, J.; Butts, C. P.; Martin, P. J.; Vergara-Gutierrez, M. C.; Heenan, R. K. *Langmuir* **2004**, *20*, 2191.
(40) Bhargava, B. L.; Klein, M. L. *Mol. Phys.* **2009**, *107*, 393.
(41) Zhu, A. L.; Wang, J. J.; Han, L. J.; Fan, M. H. *Chem. Eng. J.* **2009**, *147*, 27.
(42) Bou Malham, I.; Turmine, M. *J. Chem. Thermodyn.* **2008**, *40*, 718.
(43) Rilo, E.; Vila, J.; Pico, J.; Garcia-Garabal, S.; Segade, L.; Varela, L. M.; Cabeza, O. *J. Chem. Eng. Data* **2010**, *55*, 639.
(44) Seddon, K. R.; Stark, A.; Torres, M. J. Viscosity and density of 1-alkyl-3-methylimidazolium ionic liquids. In *Clean Solvents*; ACS Symposium Series 819; American Chemical Society: Washington, DC, 2002; p 34.
(45) Arce, A.; Rodriguez, H.; Soto, A. *Fluid Phase Equilib.* **2006**, *242*, 164.
(46) Harris, K. R.; Kanakubo, M.; Woolf, L. A. *J. Chem. Eng. Data* **2006**, *51*, 1161.
(47) Mokhtarani, B.; Mojtahedi, M. M.; Mortaheb, H. R.; Mafi, M.; Yazdani, F.; Sadeghian, F. *J. Chem. Eng. Data* **2008**, *53*, 677.
(48) Sanchez, L. G.; Espel, J. R.; Onink, F.; Meindersma, G. W.; de Haan, A. B. *J. Chem. Eng. Data* **2009**, *54*, 2803.
(49) Restolho, J.; Serro, A. P.; Mata, J. L.; Saramago, B. *J. Chem. Eng. Data* **2009**, *54*, 950.
(50) Freire, M. G.; Neves, C. M. S. S.; Marrucho, I. M.; Coutinho, J. A. P.; Fernandes, A. M. *J. Phys. Chem. A* **2010**, *114*, 3744.
(51) Sturlaugson, A. L.; Fruchey, K. S.; Lynch, S. R.; Aragon, S. R.; Fayer, M. D. *J. Phys. Chem. B* **2010**, *114*, 5350.
(52) Deeg, F. W.; Stankus, J. J.; Greenfield, S. R.; Newell, V. J.; Fayer, M. D. *J. Chem. Phys.* **1989**, *90*, 6893.
(53) Ruhman, S.; Williams, L. R.; Joly, A. G.; Kohler, B.; Nelson, K. A. *J. Phys. Chem.* **1987**, *91*, 2237.
(54) Yan, Y. X.; Nelson, K. A. *J. Chem. Phys.* **1987**, *87*, 6240.
(55) Palese, S.; Schilling, L.; Miller, R. J. D.; Staver, P. R.; Lotshaw, W. T. *J. Phys. Chem.* **1994**, *98*, 6308.
(56) Cang, H.; Li, J.; Fayer, M. D. *J. Chem. Phys.* **2003**, *119*, 13017.
(57) Cang, H.; Li, J.; Novikov, V. N.; Fayer, M. D. *J. Chem. Phys.* **2003**, *118*, 9303.
(58) Cang, H.; Novikov, V. N.; Fayer, M. D. *J. Chem. Phys.* **2003**, *118*, 2800.
(59) Nicolau, B. G.; Sturlaugson, A.; Fruchey, K.; Ribeiro, M. C.; Fayer, M. D. *J. Phys. Chem. B* **2010**, *114*, 8350.
(60) Götze, W.; Sperl, M. *Phys. Rev. Lett.* **2004**, *92*, 105701.
(61) Cang, H.; Li, J.; Andersen, H. C.; Fayer, M. D. *J. Chem. Phys.* **2005**, *123*, 64508.
(62) Li, J.; Cang, H.; Andersen, H. C.; Fayer, M. D. *J. Chem. Phys.* **2006**, *124*, 14902.
(63) Lipari, G.; Szabo, A. *Biophys. J.* **1980**, *30*, 489.
(64) Wang, C. C.; Pecora, R. *J. Chem. Phys.* **1980**, *72*, 5333.
(65) Sahu, K.; Mondal, S. K.; Ghosh, S.; Roy, D.; Bhattacharyya, K. *J. Chem. Phys.* **2006**, *124*, No. 124909.
(66) Leezenberg, P. B.; Marcus, A. H.; Frank, C. W.; Fayer, M. D. *J. Phys. Chem.* **1996**, *100*, 7646.
(67) Kivelson, D. In *Rotational Dynamics of Small and Macromolecules*; Dorfmüller, T., Pecora, R., Eds.; Springer: Berlin, 1987.
(68) Allison, S. A. *Macromolecules* **1999**, *32*, 5304.
(69) Hu, C. M.; Zwanzig, R. *J. Chem. Phys.* **1974**, *60*, 4354.
(70) Perrin, F. *J. Phys. Radium* **1934**, *5*, 497.
(71) Tirado, M. M.; Garciadelatorre, J. *J. Chem. Phys.* **1980**, *73*, 1986.
(72) Keyes, T.; Kivelson, D. *J. Chem. Phys.* **1972**, *56*, 1057.
(73) Madden, P. A.; Battaglia, M. R.; Cox, T. I.; Pierens, R. K.; Champion, J. *Chem. Phys. Lett.* **1980**, *76*, 604.
(74) Elola, M. D.; Ladanyi, B. M.; Scodinu, A.; Loughnane, B. J.; Fourkas, J. T. *J. Phys. Chem. B* **2005**, *109*, 24085.
(75) Battaglia, M. R.; Cox, T. I.; Madden, P. A. *Mol. Phys.* **1979**, *37*, 1413.
(76) Alms, G. R.; Bauer, D. R.; Brauman, J. I.; Pecora, R. *J. Chem. Phys.* **1973**, *58*, 5570.
(77) Bauer, D. R.; Alms, G. R.; Brauman, J. I.; Pecora, R. *J. Chem. Phys.* **1974**, *61*, 2255.
(78) Alms, G. R.; Bauer, D. R.; Brauman, J. I.; Pecora, R. *J. Chem. Phys.* **1973**, *59*, 5310.
(79) Fourkas, J. T.; Zhong, Q. *J. Phys. Chem. B* **2008**, *112*, 15529.
(80) Brace, D. D.; Gottke, S. D.; Cang, H.; Fayer, M. D. *J. Chem. Phys.* **2002**, *116*, 1598.
(81) Li, J.; Wang, I.; Fruchey, K.; Fayer, M. D. *J. Phys. Chem. A* **2006**, *110*, 10384.
(82) Nicolau, B. G.; Sturlaugson, A.; Fruchey, K.; Ribeiro, M. C. C.; Fayer, M. D. *J. Phys. Chem. B* **2010**, *114*, 8350.
(83) Fruchey, K.; Fayer, M. D. *J. Phys. Chem. B* **2010**, *114*, 2840.
(84) Karmakar, R.; Samanta, A. *J. Phys. Chem. A* **2002**, *106*, 6670.
(85) Shannon, M. S.; Bara, J. E. *Ind. Eng. Chem. Res.* **2011**, *50*, 8665.
(86) Shirota, H.; Fujisawa, T.; Fukazawa, H.; Nishikawa, K. *Bull. Chem. Soc. Jpn.* **2009**, *82*, 1347.
(87) Mandal, P. K.; Sarkar, M.; Samanta, A. *J. Phys. Chem. A* **2004**, *108*, 9048.
(88) Hu, Z. H.; Margulis, C. J. *Acc. Chem. Res.* **2007**, *40*, 1097.
(89) Danten, Y.; Cabaco, M. I.; Besnard, M. *J. Phys. Chem. A* **2009**, *113*, 2873.
(90) Annapureddy, H. V. R.; Hu, Z. H.; Xia, J. C.; Margulis, C. J. *J. Phys. Chem. B* **2008**, *112*, 1770.
(91) Sangoro, J.; Iacob, C.; Serghei, A.; Naumov, S.; Galvosas, P.; Karger, J.; Wespe, C.; Bordusa, F.; Stoppa, A.; Hunger, J.; Buchner, R.; Kremer, F. *J. Chem. Phys.* **2008**, 128.
(92) Li, W. J.; Zhang, Z. F.; Han, B. X.; Hu, S. Q.; Xie, Y.; Yang, G. Y. *J. Phys. Chem. B* **2007**, *111*, 6452.
(93) Kivelson, D.; Madden, P. *Mol. Phys.* **1975**, *30*, 1749.

(94) Ediger, M. D. *Annu. Rev. Phys. Chem.* **2000**, *51*, 99.